Nonlinear Dyn (2021) 103:2903–2916
https://doi.org/10.1007/s11071-021-06239-z

ORIGINAL PAPER

Deterministic and stochastic dynamics in a gene regulatory network mediated by miRNA

Lijie Hao · Zhuoqin Yang · Yuanhong Bi

Received: 30 August 2020 / Accepted: 19 January 2021 / Published online: 17 February 2021

Abstract MicroRNAs are able to modulate gene expression at the posttranscriptional level and play an essential role in various biological processes. In this paper, we establish a general model of an miRNA-mediated gene regulatory network motif with extracellular stimulus. Dynamical properties of the regulatory motif without stimulus focus on diverse codimension-1 and codimension-2 bifurcation analyses of two important feedback strengths as the parameters. Under varying levels of stimulus, we further consider stochastic dynamics controlled by crucial behaviors of monostability, bistability, excitability and oscillation in four typical regions on different two-parameter bifurcation diagrams. Furthermore, we apply potential landscapes to characterize global dynamics and stability behind physical properties of the stochastic behaviors. More essentially, our model can qualitatively simulate experimental findings of long-term memory formation in *Aplysia*.

Keywords microRNA · gene regulatory network · bifurcation · potential landscape · long-term memory

1 Introduction

MicroRNAs (miRNAs) are small non-coding RNAs as vital posttranscriptional regulators of gene expression that may be able to mediate cleavage or translational repression of their target mRNAs [1–6]. For the last several years, the regulatory roles of miRNAs have been studied both experimentally and theoretically, which revealed that miRNAs may control diverse cellular functions, including development, proliferation, metabolism, apoptosis, immunity, and, more recently, neuronal growth and plasticity [7–10]. Dysregulation of miRNAs has been implicated in many diseases such as Alzheimer's disease [11], Parkinson's disease [12] and many cancers [13]. However, the underlying mechanisms of various functions of miRNAs through biologically meaningful networks integrating multiple genes still need to be explored.

Many mathematical models have been developed to investigate dynamics of microRNA-mediated motifs [14–21]. Liu et al. [16] show that how the dynamics of two minimal architectures is drastically affected by two mechanisms of small non-coding RNAs participating in cellular processes, and a comparison is given

L. Hao
School of Mathematics Science, Tianjin Normal University, Tianjin 300387, China

Z. Yang (✉)
School of Mathematics and Systems Science and LMIB, Beihang University, Beijing 100191, China
e-mail: yangzhuoqin@buaa.edu.cn

Y. Bi
School of Statistics and Mathematics, Inner Mongolia University of Finance and Economics, Hohhot 010070, China

Y. Bi
Inner Mongolia Key Laboratory for Economic Data Analysis and Mining, Hohhot 010070, China

to reveal the implication of the fundamental differences. Zhou et al. [18] provide a general computational model for a two-node miRNA-mediated feedback loop (MFL) in which a transcriptional factor (TF) regulates an miRNA, and show that the MFL can behave either as switches and as oscillators, depending on the TF as a repressor or an activator. By using a combination of deterministic and stochastic methods, Nitzan et al. [20] present a theoretical and numerical study of coherent mixed feedback loops of two genes, in which a transcription factor and a small non-coding RNA mutually regulate each other's expression.

However, extracellular stimulus has not been concerned in the above models, which may exist in miRNA-regulated biological systems. For example, miR-124 as a memory-related microRNA can regulate long-term memory in *Aplysia* by binding to the transcription factor CREB1 (cyclic AMP (cAMP)-response element-binding protein) mRNA under the stimulation of 5-HT [7,22]. In addition, 5-HT triggers downregulation of microRNA-22 (miR-22) and thereby upregulates the expression of CPEB, which in turn regulates the presynaptic expression of atypical PKC, another candidate regulator of memory maintenance [23]. Long-term sensitization is due to long-term facilitation (LTF) of synaptic connections between sensory neurons and motor neurons, which is induced by the modulatory actions of the neurotransmitter 5-HT [24–27]. Therefore, from the viewpoint of biological significance, it is necessary to consider extracellular stimulus in mathematical modeling of miRNA-regulated systems.

Stochastic models can more accurately describe the dynamics of gene regulatory systems due to inevitable noise. The idea of potential landscapes has been introduced to uncover the global biological principles of protein dynamics, interactions, and gene networks [28–33]. For a non-equilibrium open system, which exchanges energies and information with the outside environments, the potential landscape is able to reveal insights into the global robustness and physical mechanisms of the non-equilibrium interactions [34–36]. Therefore, it is worthy of investigating the system dynamics of a stochastic model through the potential landscapes.

In this paper, we provide a mathematical model of an miRNA-mediated network motif with extracellular stimulus. We first characterize dynamical properties of the regulatory motif without stimulus through bifurcation analysis, which indicates that varying the parameters in the model can produce various codimension-1 and codimension-2 bifurcations. Then, deterministic and stochastic dynamics in the system with changing stimulus reveal that the stochastic dynamics of the system is consistent with the deterministic dynamics. These dynamics of monostability, bistability, excitability and oscillation are further examined by means of the potential landscape. In addition, we show that the model can qualitatively simulate several experimental findings of long-term memory formation in *Aplysia*.

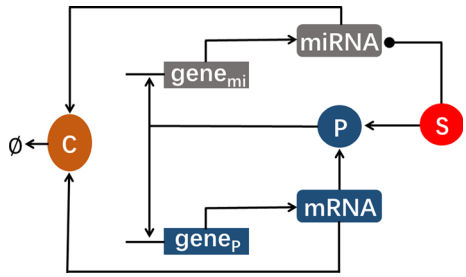

Fig. 1 Schematic description of our model. Protein (P) is activated, while miRNA is repressed by stimulus (S). P activates the miRNA gene and its own gene transcription. mRNA and miRNA are combined into a complex (C)

2 Model and method

2.1 Model development

We develop a network motif with extracellular stimulation to describe the interplay of an miRNA, an mRNA and a protein, as shown in Fig. 1. Protein (P), as a transcriptional activator, activates miRNA gene ($gene_{mi}$) but is negatively regulated by miRNA (grey), and P would also activate expression of its own gene ($gene_P$) to form a positive feedback loop (blue). Furthermore, we assume that an extracellular stimulus (S) can activate the P and downregulate the miRNA level. The miRNA and the mRNA are combined into a complex (C) with a rate of δ, which is assumed to be degraded rather than dissociated into its miRNA and mRNA components.

We denote the concentrations of the stimulus, the miRNA, the mRNA and the P as [S], [miRNA], [mRNA] and [P], respectively. The extracellular stimulus S is considered by defining linear functions λ[S] [miRNA] in equation (1) for inhibition on miRNA

Table 1 Default parameter values of eqs. (1)–(3)

Parameter	Value	Parameter	Value
[S] (μM)	0	λ (μM^{-1} min^{-1})	0.001
V_1 (μM min^{-1})	7	V_2 (μM min^{-1})	5
K_1 (μM)	5	K_2 (μM)	5
k_s (min^{-1})	0.001	γ (min^{-1})	0.2
g_m (μM min^{-1})	0.06	g_i (μM min^{-1})	0.75
d_p (min^{-1})	0.06	d_i (min^{-1})	0.02
d_m (min^{-1})	0.02	δ (μM^{-1} min^{-1})	0.02

and k_s[S] in equation (3) for protein activation under the stimulation of S. The roles of the protein in gene expression are represented by Hill type functions of [P] with Hill coefficients of 2, in which transcription of miRNA gene and its own gene can be described as $\frac{V_1[\mathrm{P}]^2}{[\mathrm{P}]^2+{K_1}^2}$ and $\frac{V_2[\mathrm{P}]^2}{[\mathrm{P}]^2+{K_2}^2}$, respectively. V_1 and V_2 are feedback strengths between miRNA and mRNA genes with sufficient P, and K_1 and K_2 are two dissociation constants of two complexes of P from promoter regions of the miRNA and mRNA genes, respectively. g_i and g_m illustrate basic transcription rates of the miRNA and mRNA genes. Degradation rates of miRNA, mRNA, and P are defined by d_i, d_m and d_p, respectively.

Here, we describe dynamics of the model using rate eqs. (1)–(3). All parameters and their basal values are listed in Table 1. In the following numerical simulations, bifurcation analyses are performed with XPPAUT, and differential equations are solved using the Runge–Kutta method [37].

$$\frac{d[\mathrm{miRNA}]}{dt} = g_i + \frac{V_1[\mathrm{P}]^2}{[\mathrm{P}]^2 + {K_1}^2} - \delta[\mathrm{miRNA}][\mathrm{mRNA}] - d_i[\mathrm{miRNA}] - \lambda[\mathrm{S}][\mathrm{miRNA}], \quad (1)$$

$$\frac{d[\mathrm{mRNA}]}{dt} = g_m + \frac{V_2[\mathrm{P}]^2}{[\mathrm{P}]^2 + {K_2}^2} - d_m[\mathrm{mRNA}] - \delta[\mathrm{miRNA}][\mathrm{mRNA}], \quad (2)$$

$$\frac{d[\mathrm{P}]}{dt} = \gamma[\mathrm{mRNA}] + k_s[\mathrm{S}] - d_p[\mathrm{P}]. \quad (3)$$

2.2 Potential landscapes

Biologically, external stochastic fluctuations from highly dynamical and inhomogeneous cellular environments can be significant for dynamics. Therefore, it needs to develop a probabilistic description to model the corresponding cellular process, which can be realized by constructing a diffusion equation on the external fluctuations for probability evolution [31,38,39].

The generalized potential is closely associated with the steady-state probability of a non-equilibrium network [31]. Landscape ideas based on a quasi-equilibrium assumption with known potentials were introduced for uncovering global principles in biology. For a non-equilibrium open system, the global dynamics and stability are determined by the potential landscape, when the landscape reflects directly the steady-state probability distribution by the weight of each state [30–35].

The dynamical equation of our model can be written as $\dot{\mathbf{X}} = \mathbf{F}(\mathbf{X})$, where $\mathbf{X} = ([\mathrm{miRNA}], [\mathrm{mRNA}], [\mathrm{P}])$, and $\mathbf{F}(\mathbf{X})$ represents the right-hand side of equations (1)-(3). Furthermore, our stochastic model due to inevitable fluctuations can more accurately extended as

$$\dot{\mathbf{X}} = \mathbf{F}(\mathbf{X}) + \zeta, \quad (4)$$

where ζ is often assumed as Gaussian white noise with its mean and variance $\langle\zeta(t)\rangle = 0$ and $\langle\zeta(t)\zeta(t')\rangle = 2\mathbf{D}\delta(t-t')$. $\mathbf{D}$ is the diffusion coefficient tensor (matrix) measuring level of the noise.

According to the stochastic process, we can get the probability of system state $P(\mathbf{X}, t)$, which evolves following the Fokker-Plank equation $\frac{\partial P}{\partial t} + \nabla \cdot \mathbf{J}(\mathbf{X}, t) = 0$, where the flux vector $\mathbf{J}$ defined as $\mathbf{J}(\mathbf{X}, t) = \mathbf{F}P - \mathbf{D} \cdot \frac{\partial}{\partial \mathbf{X}} P$ measures the speed of the flow in the concentration space. If the system reaches the steady state, $\frac{\partial P}{\partial t} = 0$ and $\nabla \cdot \mathbf{J}(\mathbf{X}, t) = 0$. Namely, the divergence of the probability flux $\mathbf{J}$ must vanish at the steady state. Thereby, there are two possibilities: one is $\mathbf{J} = 0$; that is, the system satisfies the detailed balance condition, the other is $\mathbf{J} \neq 0$; that is, the detailed balance condition is broken and the system stays at non-equilibrium state.

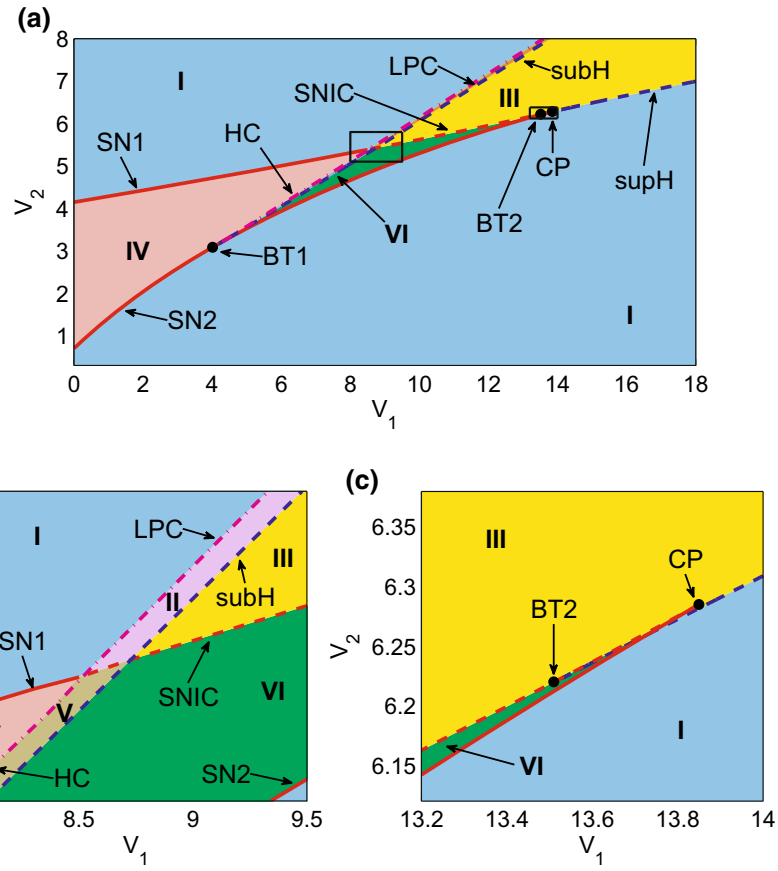

Fig. 2 Bifurcation diagram in the (V_1, V_2) parameter plane when [S] $= 0$ μM. The red solid line, red dashed line, blue dashed line and magenta dash-dotted line depict the saddle-node bifurcation points (SN), saddle-node invariant circle bifurcation points (SNIC), Hopf bifurcation points (supH and subH) and fold limit cycle bifurcation points (LPC) (or homoclinic bifurcation points (HC)), respectively. These loci delineate six regions denoted by regions I–VI. Two codimension-2 bifurcation points exist: a cusp point (CP) and a Bogdanov–Takens bifurcation point (BT). The rectangles in **a** indicate the regions that are enlarged in **b** and **c**

Based on the definition, the probability flux at the steady state can be given by

$$\mathbf{J}_{ss} = \mathbf{F} P_{ss} - \mathbf{D} \cdot \frac{\partial}{\partial \mathbf{X}} P_{ss}, \tag{5}$$

where P_{ss} is the stationary state probability, and $U = -\ln P_{ss}$ is defined as the non-equilibrium potential related with the stationary state probability.

3 Results

3.1 Dynamics of the regulatory motif without stimulus

We first aim to reveal the regulatory mechanism for the protein and the miRNA in our model by setting [S] $= 0$ μM (see Fig. 1). Since the parameters V_1 and V_2 measure the feedback strength of miRNA activation by P and the strength of self-induced activation of the P, we focus on bifurcations in the system by adjusting the values of these two parameters (see Fig. 2). Five different types of codimension-1 bifurcation points are found, namely, saddle-node bifurcation points (SN), saddle-node invariant circle bifurcation points (SNIC), supercritical and subcritical Hopf bifurcation points (supH and subH), fold limit cycle bifurcation points (LPC) and homoclinic bifurcation points (HC). Then, two-parameter bifurcation diagram in the (V_1, V_2) plane is constructed by continuation of the loci of these codimension-1 bifurcation points, as shown in Fig. 2. The SN1 and SN2 bifurcation curves (red solid line) coalesce at a codimension-2 cusp point (CP), whereas they meet with the subH and the supH bifurcation curves (blue dashed) at two codimension-2 Bogdanov–Takens bifurcation points (BT1 and BT2), respectively. The upper section of the magenta dash-dotted curve is composed of the LPC bifurcation point that gives rise to the stable and the unstable limit cycle. Instead, the HC bifurcation point is generated on the lower section of the magenta dash-dotted curve, when the only existing unstable limit cycle before encounter-

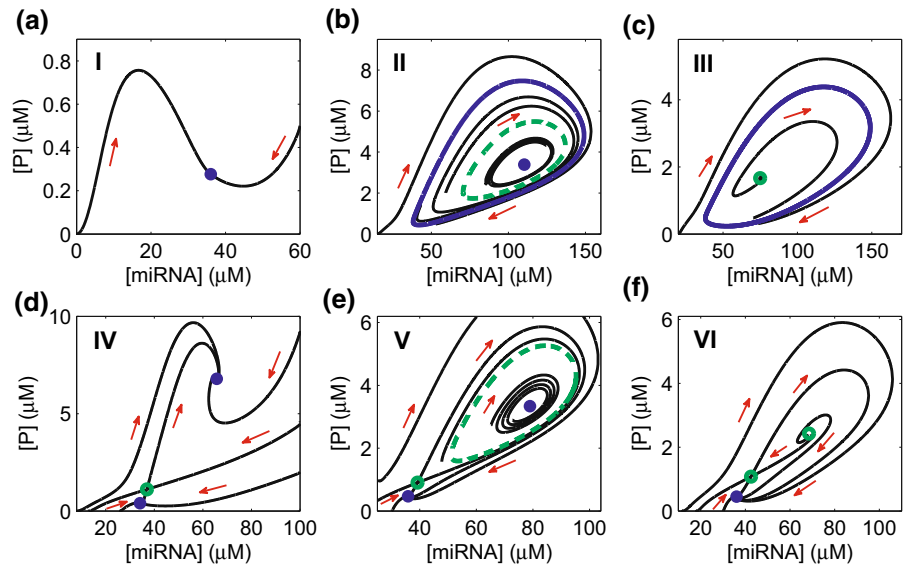

Fig. 3 Phase diagrams corresponding to the six labeled regions in Fig. 2. **a** $(V_1, V_2) = (10, 0.5)$. **b** $(V_1, V_2) = (11.75, 7)$. **c** $(V_1, V_2) = (15, 7)$. **d** $(V_1, V_2) = (5, 4.1)$. **e** $(V_1, V_2) = (7.82, 5)$. **f** $V_1, V_2) = (8.5, 5)$. Stable (unstable) steady states are denoted by blue solid (green open) circles and stable (unstable) limit cycle by blue solid (green dashed) curves. Black curves correspond to deterministic trajectories of the system with diverse initial values

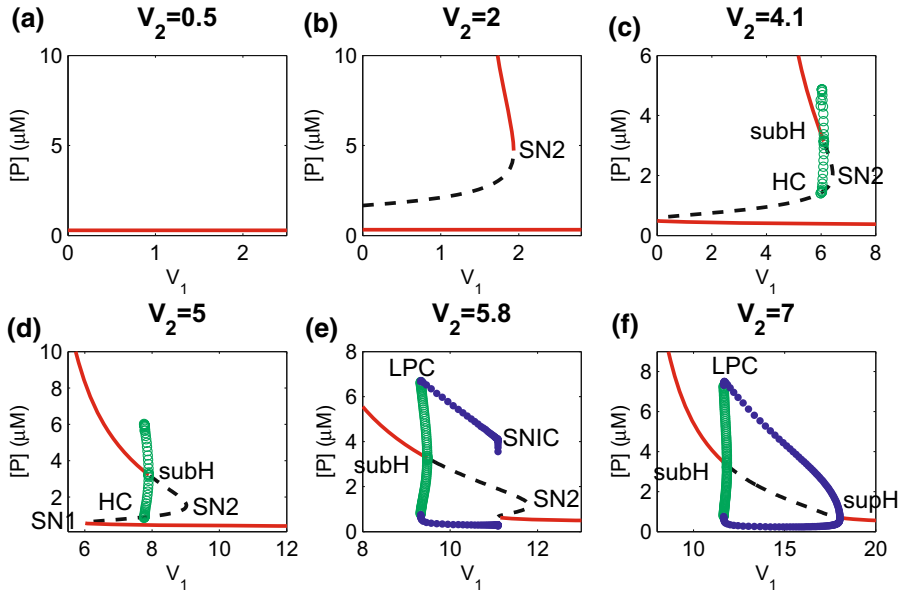

Fig. 4 Bifurcation diagrams of [P] versus V_1 at six values of V_2 when [S] $= 0\ \mu M$. Stable and unstable steady states are represented by red solid lines and black dashed lines, respectively. For the stable and unstable limit cycles, the maximum and minimum values of [P] are denoted by blue solid circles and green open circles, respectively. Bifurcation points are marked as SN, saddle-node bifurcation point; supH, supercritical bifurcation point; subH, subcritical bifurcation point; HC, homoclinic bifurcation point; LPC, fold limit cycle bifurcation point; and SNIC, saddle-node invariant circle bifurcation point

ing the LPC bifurcation curve collides with the saddle between the SN1 and SN2 bifurcation curves.

The (V_1, V_2)-parameter plane is further divided into six regions as I–VI by the curves of different bifurcation types in Fig. 2. Six phase diagrams of dynamic solutions for [P] and [miRNA] illustrated in Fig. 3 facilitate perceptual understanding of distinctive dynamic behaviors of these six regions. Now, we attempt to classify all the regions by qualitative properties of the number of steady states decided by the SN1 and SN2 bifurcation curves as well as appearance and disappearance of limit cycles.

Monostability in the region I is determined by a lower stable steady state below the SN2 bifurcation curve or a higher stable steady state above the SN1 bifurcation curve as shown in Fig. 3**a**. The higher stable steady state is surrounded by a stable limit cycle and an unstable limit cycle in the region II (see Fig. 3b) via the LPC bifurcation curve. Furthermore, the unstable limit cycle disappears, but the stable limit cycle exists as oscillation in region III (see Fig. 3c) via the subH bifurcation curve. Otherwise, two steady states coexist with a saddle in the regions IV, V and VI between the SN1 and the SN2 bifurcation curves. The region IV is characterized in bistability when these two stable steady states coexists with the saddle (see Fig. 3d). Nevertheless, the higher stable steady state is surrounded by an unstable limit cycle in the region V (see Fig. 3e). As the parameters pass through the subH bifurcation curve, the higher stable steady state loses stability and becomes unstable in the region VI. All those makes the system become excitable in the regions V and VI (see Fig. 3f).

To better understand transition mechanisms of the different regions in Fig. 2, we choose six values of V_2 to display qualitatively different one-parameter bifurcation diagrams of [P] versus V_1 as shown in Fig. 4. For a small value of V_2 as 0.5, the system invariably lying in the region I in Fig. 2 has to keep monostable (see Fig. 4a). As V_2 is increased to 2 and even 4.1 (see Fig. 4b), the system makes change from bistability to monostability with the increasing V_1 via a saddle-node bifurcation (SN2) on the SN2 bifurcation curve in Fig. 2 (see Fig. 4b and c). Only difference of them is that an unstable limit cycle generated by a subcritical Hopf bifurcation (subH) on the upper branch grows gradually and then collides with a saddle at a homoclinic bifurcation (HC) point on the middle branch in Fig. 4c. Bifurcation behaviors for $V_2 = 5$ (see Fig. 4d) experience a transition from a high stable steady state with monostability to three steady states via a saddle-node bifurcation (SN1) and further to a low stable steady state with monostability via another saddle-node bifurcation (SN2), accompanied with an unstable limit cycle via the bifurcations the same as that in Fig. 4c. As V_2 is fixed at 5.8 (see Fig. 4e) and 7 (see Fig. 4f), stable limit cycles and unstable limit cycles appear pairwise around only stable steady states via fold limit cycle bifurcations (LPC). Furthermore, the unstable limit cycles shrink as well as the stable steady states loses stability through a subcritical Hopf bifurcation (subH) with increasing V_1. However, different destinies of the stable limit cycles are that it vanishes via SNIC bifurcations in Fig. 4e, while it shrinks to a supercritical Hopf bifurcation (supH) point in Fig. 4f.

In summary, with respect to these two parameters V_1 and V_2 associated with modulations of miRNA and P, our model enables to provide abundant dynamical properties such as monostability, bistability, excitability and oscillations, which themselves can make different transitions via complex bifurcation mechanisms as shown in the codim-1 and codim-2 bifurcation diagrams.

3.2 Deterministic and stochastic dynamics under changeable levels of stimulus

Extracellular stimulus exists in miRNA-regulated systems and noise is inevitably involved in biological processes, both of which have not been considered in previous models. Now, we will consider deterministic and stochastic dynamics in the system under varying levels of the stimulus S. Based on the bifurcation analysis of V_1 at the six typical values of V_2 as above in Sect. 3.1, we further construct codim-2 bifurcation diagrams in parameters plane (V_1, [S]) in Fig. 5 to give a comparison before and after stimulation.

The monostability in Fig. 4a is still able to cover very large region even under stimulation, although enough large amount of the stimulus S leads to appearance of a narrow bistable region in Fig. 5a. Even the bistable region in Fig. 4b is accessible to become monostable after stimulation in Fig. 5b. All those suggest that the monostable state with strong stability is relative robust to the stimulus. However, for the bistable states surrounded by the unstable limit cycles in Fig. 4c and d, the increasing stimulation leads to expansions of oscillatory regions for stable limit cycles and excitable regions

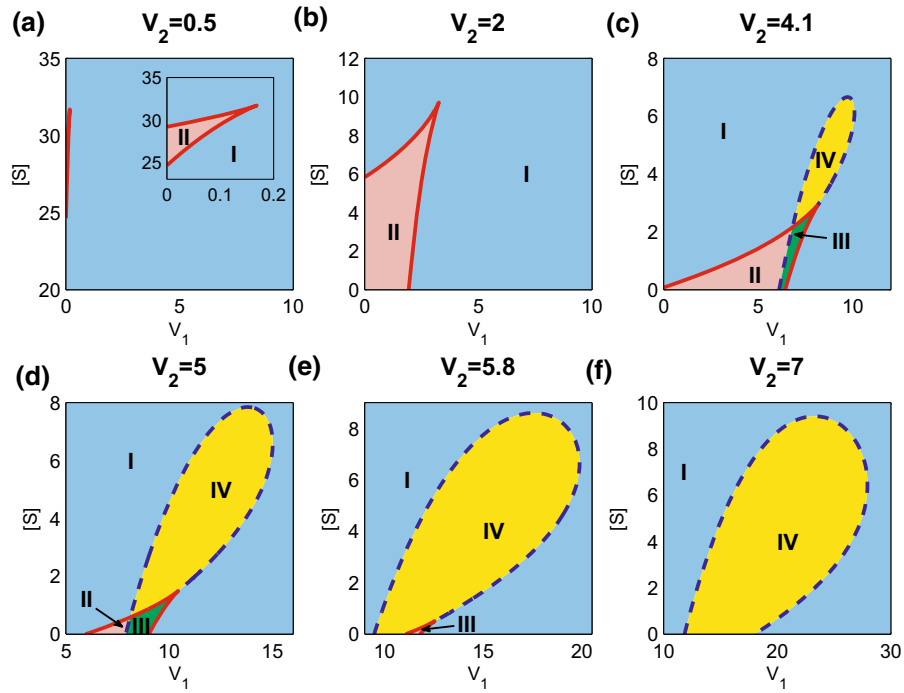

Fig. 5 Bifurcation diagrams in the $(V_1, [S])$-parameter plane at different values of V_2. Red solid and blue dashed lines depict the loci of saddle-node bifurcation points and Hopf bifurcation points, respectively. These loci delineate four regions: monostable region, bistable region, excitable region and oscillatory region, which are denoted by regions I, II, III and IV, respectively

for unstable steady states but contraction of bistable regions as shown in Fig. 5c and d. For the stable limit cycle existing without stimulation in Fig. 4e and f, the oscillatory regions become larger and larger in Fig. 5e and f under the control of the stimulus. Indeed, monostability, bistability, excitability and oscillation are the crucial dynamical behaviors in modeling often used to explicate physical phenomena such as state transition and biological rhythms.

Furthermore, as an inevitable existence of noise in biological systems, stochastic model can more accurately describe the dynamics of the system. Therefore, stochastic dynamics of the gene regulatory network with noise (Eq. (1)) is discussed in the four typical dynamics behaviors including monostability and bistability for small V_2 in Fig. 5b, monostability, bistability, excitability and oscillation for moderate V_2 in Fig. 5d, and only oscillations for large V_2 in Fig. 5f as follows.

3.2.1 Stochastic dynamics controlled by monostability and bistability at small value of V_2

The $(V_1, [S])$-parameter plane is divided into two regions I and II by the loci of saddle-node bifurcation points for the small $V_2 = 2$ in Fig. 5b, that is, a monostable region I with a single stable steady state and a bistable region II with two stable steady states and a saddle. Also, deterministic and stochastic phase diagrams of the two labeled regions are illustrated in Fig. 6, where the concentrations of both miRNA and protein ([miRNA] and [P]) reside near the monostable steady state in Fig. 6a but stochastically transit between the high and the low stable steady states in Fig. 6b.

To explore global stochastic dynamics from the potential perspective, we projected the potential function onto two independent variables, i.e., the miRNA concentration [miRNA] and the protein concentration [P]. On the potential landscapes for parameter values from the two typical regions I and II, only one basin of attraction corresponds to the global stable steady state in the monostable region I (see Fig. 7a), while two funnels toward the local minima corresponds to the high and the low stable states in the bistable region II (see Fig. 7b).

3.2.2 Stochastic dynamics governed by monostability, bistability, excitability and oscillation at moderate value of V_2

Figure 5d illustrates that the $(V_1, [S])$-parameter plane is divided into four regions as depicted by regions I–IV by the loci of saddle-node bifurcation points and Hopf

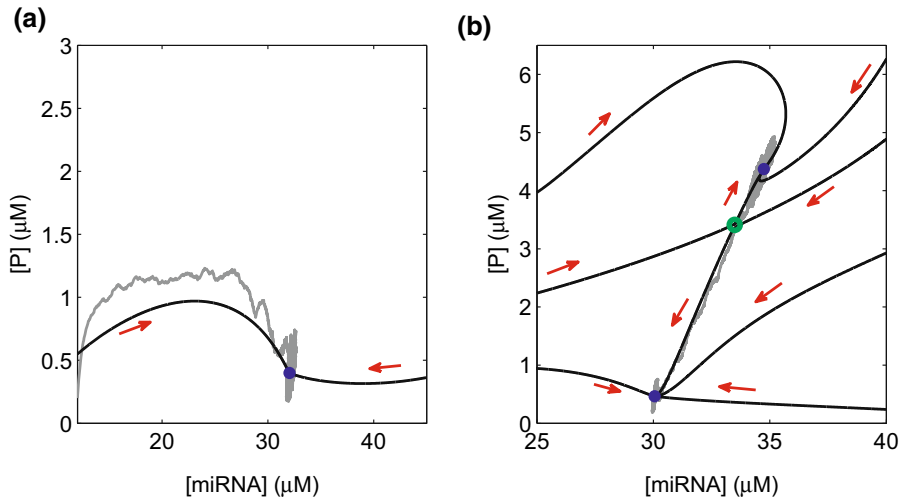

Fig. 6 Deterministic and stochastic phase diagrams corresponding to the regions I and II in Fig. 5b. Stable (unstable) steady states are denoted by blue solid (green open) circles. Black curves correspond to deterministic trajectories of the system with diverse initial values. Gray curves correspond to stochastic trajectories with a noise strength $D = 0.0002$

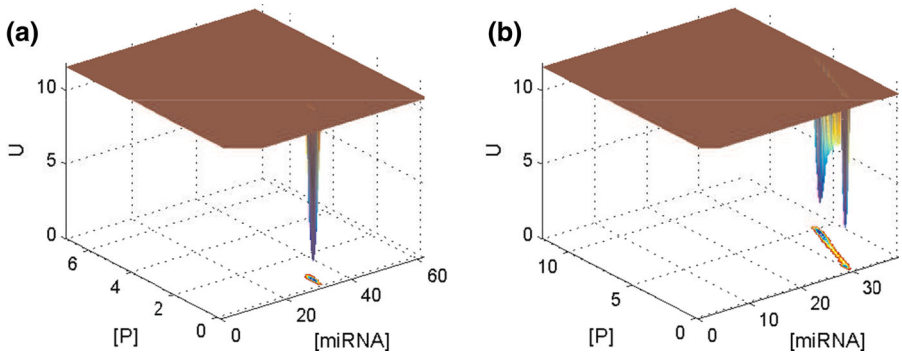

Fig. 7 The potential landscapes for the stochastic dynamics in Fig. 6. The parameters are the same as those in the phase diagrams of Fig. 6, and the diffusion matrix was taken as the diagonal matrix with a noise strength $D = 0.0002$

bifurcation points at moderate $V_2 = 5$. The system is monostable with a single stable steady state in the region I, but bistable with two stable steady states and a saddle in the region II. Region III behaves excitable with a stable steady state, an unstable steady state and a saddle while region IV has large oscillation of a stable limit cycle around an unstable steady state.

Several typical deterministic and stochastic dynamics as well as potential landscape in the four labeled regions are illustrated in Figs. 8 and 9 , respectively. Some small fluctuations different from that in Fig. 6a arise from the change of the property of the only stable steady state from the node to the focus in Fig. 8a. Also, the potential landscape in Fig. 9a shows that the potential with more broader area than that in Fig. 7a is funneled toward a global minimum corresponding to the global stable steady state. Stochastic transition between two stable steady states in the bistable region II is caused by the noise forcing the system into either of their attracting basins (see Fig. 8b). However, attractor region of the stable focus restricted by stable and unstable manifolds of saddle is much larger than that of the stable node. Therefore, most of stochastic orbits after experiencing a large journey rotate around the stable focus. Two stable steady states in the region II decide that the potential has two local minima for high and low levels of miRNA and protein, respectively (see Fig. 9b). Moreover, projection sizes of the two minima are apparently different on the ([miRNA], [P]) plane.

Furthermore, the stable focus becomes unstable, which leads to the excitable region III when a lower stable steady state coexists along with an unstable one and a saddle in Fig. 8c. Noise gives rise to a large excursion of the miRNA and protein concentrations around the unstable focus and then pull it toward the stable steady state at low concentration levels. Eventually, the potential landscape exhibits a deep funnel toward a global minimum corresponding to the global stable steady state as well as a valley that corresponds to the excitable trajectories around the unstable focus (see

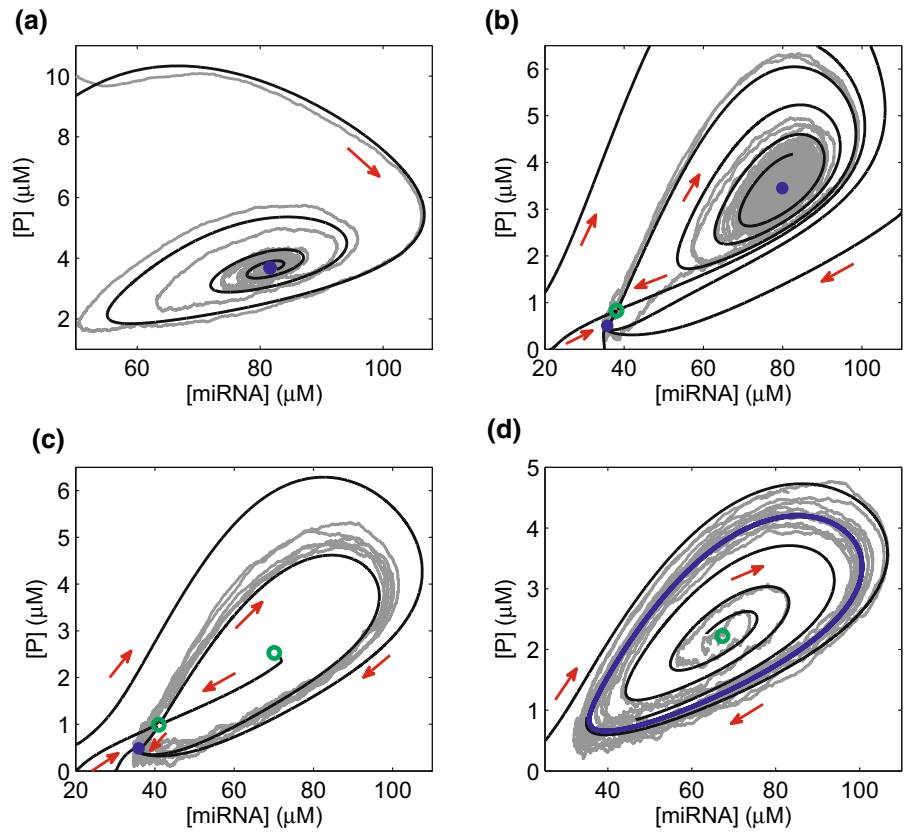

Fig. 8 Deterministic and stochastic phase diagrams corresponding to the regions I–IV in Fig. 5d. Stable (unstable) steady states are denoted by blue solid (green open) circles and stable limit cycle by blue solid curves. Black curves correspond to deterministic trajectories of the system with diverse initial values. Gray curves correspond to stochastic trajectories with a noise strength $D = 0.0002$

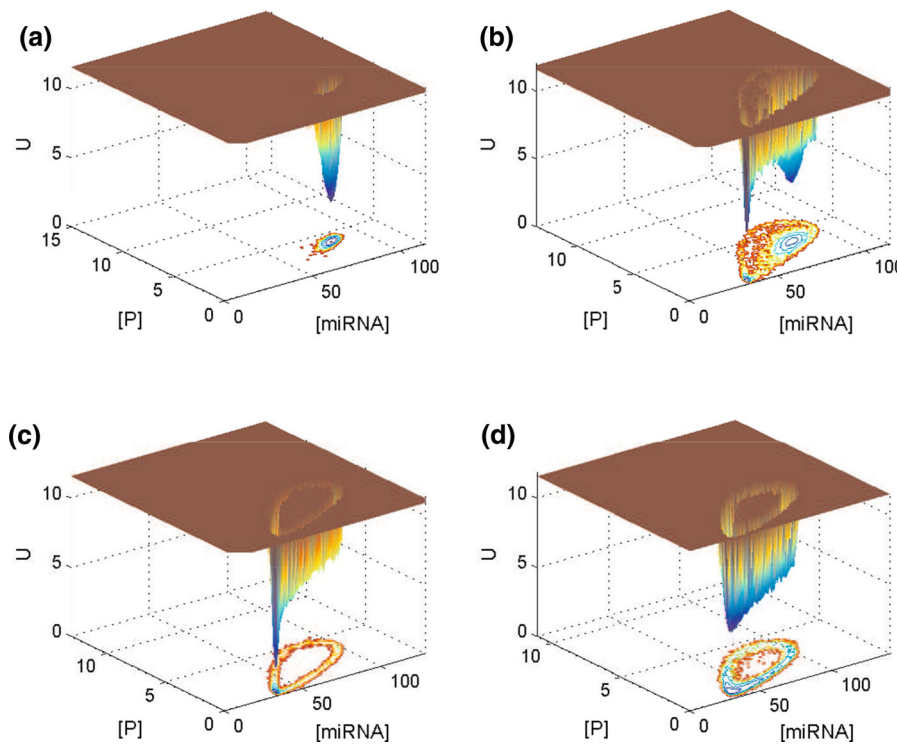

Fig. 9 The potential landscapes for the stochastic dynamics in Fig. 8. The parameters are the same as those in the phase diagrams of Fig. 8, and the diffusion matrix was taken as the diagonal matrix with a noise strength $D = 0.0002$

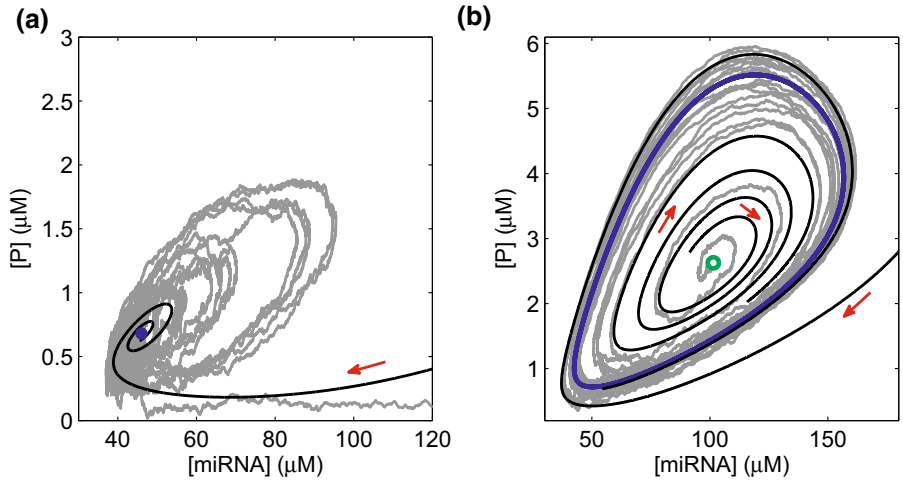

Fig. 10 Deterministic and stochastic phase diagrams corresponding to the regions I and II in Fig. 5f. Stable (unstable) steady states are denoted by blue solid (green open) circles and stable limit cycle by blue solid curves. Black curves correspond to deterministic trajectories of the system with diverse initial values. Gray curves correspond to stochastic trajectories with a noise strength $D = 0.0002$

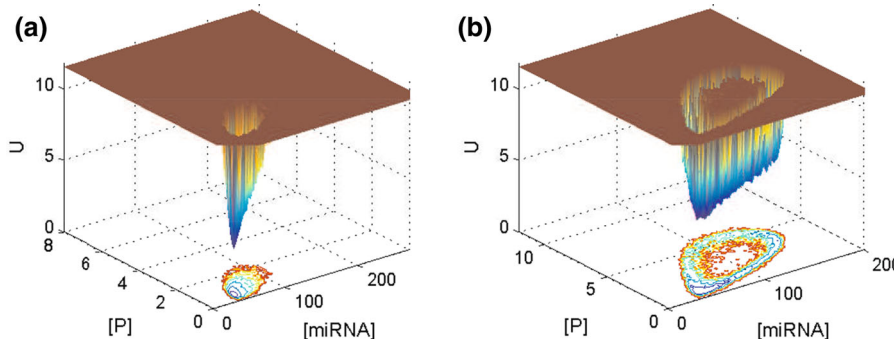

Fig. 11 The potential landscapes for the stochastic dynamics in Fig. 10. The parameters are the same as those in the phase diagrams of Fig. 10, and the diffusion matrix was taken as the diagonal matrix with a noise strength $D = 0.0002$

Fig. 9c). However, the appearance of a stable limit cycle makes stochastic trajectory due to noise move rapidly toward it and then oscillates around it in Fig. 8d, and so the potential landscape exhibits a closed ring valley corresponding to the stable limit cycle (see Fig. 9d).

3.2.3 Oscillations with gradually large amplitude for large V_2

As $V_2 = 7$, there are the monostable region I with a single stable steady state and the oscillatory region IV with a stable limit cycle around an unstable steady state separated by the loci of Hopf bifurcation points (see Fig. 5f). Typical deterministic and stochastic dynamics shows small fluctuations near the monostable steady state in Fig. 10a but gradually large oscillation around the stable limit cycle in Fig. 10b. Here, small fluctuations appearing near the stable steady state in Fig. 10 a are decided by properties of the focus, even though the potential is still funneled toward a global minimum corresponding to the global stable steady state (see Fig. 11a). However, the gradually large oscillation around the stable limit cycle in Fig. 10b is represented as irregular and inhomogeneous closed ring valley on the potential landscape in Fig. 11b.

3.3 The model can qualitatively simulate experimental findings of long-term memory formation in *Aplysia*

Empirically, treatment of five pulses with 5-HT induce long-term facilitation of synapses between *Aplysia* sensory neurons and motor neurons, whereas that of three pules do not. Interval applications of five pulses of 5-HT to the sensory neurons reduced the expression of miR-124 and increased CREB1 protein levels [7]. Additionally, there are several putative CREB binding sites in the presumed promoter region upstream of the *Aplysia* miR-124 gene, and biologists have suggested that CREB may be able to regulate miR-124 expression levels [7]. Thus, we assume that the transcriptional activator CREB1 promotes miR-124 gene transcription. As

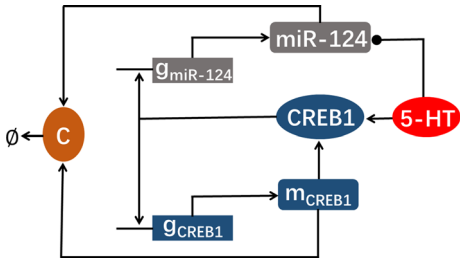

Fig. 12 Illustration of the model for the miRNA-mediated gene regulatory network in *Aplysia*. The protein (CREB1) is activated, while miR-124 is repressed by the stimulus (5-HT). CREB1 activates the miR-124 gene and its own gene transcription. CREB1 mRNA (m_{CREB1}) and miR-124 are combined into a complex (C)

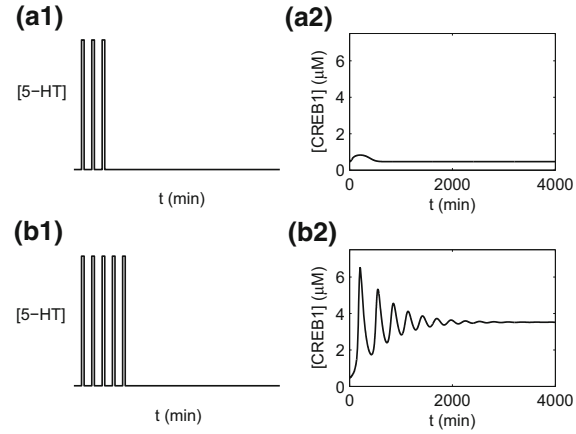

Fig. 13 Time courses of [CREB1] (the second column) under different stimulus protocols (the first column) at $V_1 = 7.7$: three pulses (a) and five pulses (b) of 10 μM stimulus for 5 min and the inter-pulse interval (from the end of one pulse to the onset of the next) of 15 min. Other parameter values are given in Table 1

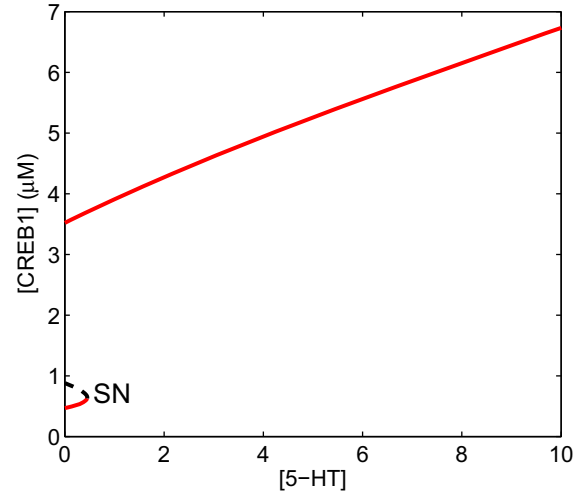

Fig. 14 Bifurcation diagram of [CREB1] versus [5-HT] at $V_1 = 7.7$. The stable and unstable states are represented by red solid lines and black dashed lines, respectively. Saddle-node bifurcation point is marked as SN. Other parameter values are given in Table 1

was mentioned above, the miRNA-mediated gene regulatory network, in which CREB1 activates the miR-124 (miRNA) gene, but CREB1 is negatively regulated by miR-124, can be described by our model shown in Fig. 1. The stimulus, the miRNA and the protein in our model are represented as 5-HT, miR-124 and transcriptional activator CREB1 in *Aplysia*, respectively (see Fig. 12), so dynamics of the network motif in *Aplysia* can be described by using rate Eqs (6)–(8).

$$\frac{d[\text{miR-124}]}{dt} = g_i + \frac{V_1[\text{CREB1}]^2}{[\text{CREB1}]^2 + {K_1}^2} - d_i[\text{miR-124}] - \delta[\text{miR-124}][\text{m}_{\text{CREB1}}] - \lambda[\text{5-HT}][\text{miR-124}], \quad (6)$$

$$\frac{d[\text{m}_{\text{CREB1}}]}{dt} = g_m + \frac{V_2[\text{CREB1}]^2}{[\text{CREB1}]^2 + {K_2}^2} - d_m[\text{m}_{\text{CREB1}}] - \delta[\text{miR-124}][\text{m}_{\text{CREB1}}], \quad (7)$$

$$\frac{d[\text{CREB1}]}{dt} = \gamma[\text{m}_{\text{CREB1}}] + k_s[\text{5-HT}] - d_p[\text{CREB1}], \quad (8)$$

where [miR-124], [m_{CREB1}] and [CREB1] denote the concentrations of miR-124, CREB1 mRNA and CREB1 in the cell, respectively.

Our model can qualitatively simulate experimental findings concerning stimulus protocols that can lead to long-term memory formation in *Aplysia* (see Fig.13). Two protocols for three (a) and five (b) short pulses, as presented in Fig.13, are applied in our model to simulate the experimental results. Three pulses of stimulus 5-HT induce a transient increase in the CREB1 protein concentration, which then returns to its original level after stimulation as shown in Fig.13a. However, five pulses of stimulus induce a persistent high level of the CREB1 protein (see Fig.13 b), which is consistent with the experimental findings.

According to the one-parameter bifurcation diagram in Fig. 14, there exists a one-way irreversible switch induced by a transition from the bistability to the monostability with increasing stimulus concentration. There are two steady states (a low and a high) in the system at [5-HT] = 0μM, and only a single high steady state at [5-HT] = 10μM. Five pulses of 10μM stimulus, but not three short pulses, are accumulated to elevate the protein concentration over a threshold to the attraction domain of the high stable steady state. Since the system is monostable at [5-HT] = 10μM, the irreversible switch can ensure that the high protein

concentration always stays at the high steady state even after the stimulation.

4 Discussion

The interplay of miRNAs, mRNAs, and proteins has been demonstrated to play crucial roles in almost all cellular processes. In the paper, we establish the generic network model of the regulation between the miRNA and the protein under the extracellular stimulus. We firstly focus on the regulatory mechanisms between the protein and the miRNA without the stimulus and perform the detailed codim-1 and codim-2 bifurcation analyses by changing the strengths of the positive and the negative feedbacks. The codim-2 bifurcation plane with the cusp and the Bogdanov–Takens points is divided into several regions by the codim-1 bifurcations curves of saddle-node, Hopf, homoclinic, fold limit cycle and saddle-node invariant circle. Also, complex transitions mechanisms of the regions of monostability, bistability, excitability and oscillations are discerned by the codim-1 and codim-2 bifurcation analyses. Furthermore, we consider deterministic and stochastic dynamics under the varying levels of the stimulus as well as noise inevitably in biological processes. The stimulation level as another parameter is added to construct the codim-2 bifurcation diagrams, and then, stochastic dynamics are discussed in the three chosen parameter diagrams with the coexistence of monostability and bistability, of monostability, bistability, excitability and oscillation, and of only oscillations, respectively. Additionally, stochastic phase diagrams in the four typical regions illustrate that the stochastic dynamics of the system is consistent with the deterministic dynamics. These results are further verified by the potential landscapes, which clearly illustrate the transitions of landscapes with changing parameter values taken from the four typical regions.

The model qualitatively simulates experimental findings of long-term memory formation in *Aplysia*, when the stimulus, miRNA and protein are represented as 5-HT, miR-124 and the transcriptional activator CREB1 in *Aplysia*, respectively. In our simulations, five pulses of stimulus induce persistent high CREB1 level for the LTM formation, whereas three pulses do not. Our results are in accordance with the experimental findings that five pulses of treatment with 5-HT, but not three, induce long-term synaptic facilitation of synapses between *Aplysia* sensory neurons and motor neurons. From the view point of dynamics, the irreversible switch on the bifurcation diagram ensures that the high protein concentration always stays at the high steady state even after the stimulation.

Previous studies [16,18] have provided computational models for investigating mechanisms and roles of miRNAs and explored dynamics by using bifurcation analyses. However, comprehensive codimension-2 bifurcation analysis and potential landscapes for stochastic dynamics, which are taken into account significantly in this work, have not been discussed in these previous studies. In addition, our model describes a gene regulatory network mediated by miRNA with extracellular stimulus, which has not been concerned in previous mathematical models for miRNA-mediated motifs. The mathematical model proposed in the paper can be used to elucidate the significant dynamic property for long-term memory formation in *Aplysia* associated with bistability. However, in some other biological systems, miRNAs can also induce more behaviors than bistability. For example, an miR-17-92 cluster can generate large-amplitude oscillations in a cancer network [40], and the accumulation of four *Arabidopsis* miRNAs (miR-171, miR-398, miR-168 and miR-167) oscillated during the diurnal cycle [41]. Therefore, more biological applications of other dynamic properties in mathematical models for gene regulatory networks mediated by miRNAs will be studied in future works.

Acknowledgements This work is supported by the National Natural Science Foundation of China with Grant No. 11902221 (LH), Nos. 11872084, 11932003 (ZY) and No. 11702149 (YB).

Author contributions LH and ZY designed and performed the research; YB and LH were responsible for programming; and ZY and LH wrote the article.

Compliance with ethical standards

Conflicts of interest All the authors declare that there is no any conflict with the publication of this work.

References

1. Lagos-Quintana, M., Rauhut, R., Lendeckel, W., Tuschl, T.: Identification of novel genes coding for small expressed RNAs. Science **294**(5543), 853–858 (2001)
2. Bartel, D.P.: MicroRNAs: genomics, biogenesis, mechanism, and function. Cell **116**(2), 281–297 (2004)

3. Filipowicz, W., Bhattacharyya, S.N., Sonenberg, N.: Mechanisms of post-transcriptional regulation by microRNAs: are the answers in sight? Nat. Rev. Genet. **9**, 102–114 (2008)
4. Bartel, D.P.: MicroRNAs: target recognition and regulatory functions. Cell **136**(2), 215–233 (2009)
5. Treiber, T., Treiber, N., Meister, G.: Regulation of microRNA biogenesis and its crosstalk with other cellular pathways. Nat. Rev. Mol. Cell Biol. **20**, 5–20 (2019)
6. Motta, F., Carena, M.C., Selmi, C., Vecellio, M.: MicroRNAs in ankylosing spondylitis: function, potential and challenges. J. Transl. Autoimmun. **3**, 100050 (2020)
7. Rajasethupathy, P., Fiumara, F., Sheridan, R., Betel, D., Puthanveettil, S.V., Russo, J.J., Sander, C., Tuschl, T., Kandel, E.R.: Characterization of small RNAs in Aplysia reveals a role for miR-124 in constraining synaptic plasticity through CREB. Neuron **63**(6), 803–817 (2009)
8. Ryan, B., Joilin, G., Williams, J.M.: Plasticity-related microRNA and their potential contribution to the maintenance of long-term potentiation. Front. Mol. Neuro. **8**, 4 (2015)
9. Liu, R., Chen, Y., Shou, T., Hu, J., Qing, C.: miRNA-99b-5p targets FZD8 to inhibit non-small cell lung cancer proliferation, migration and invasion. OncoTargets Ther. **12**, 2615–2621 (2019)
10. Channakkar, A.S., Singh, T., Pattnaik, B., Gupta, K., Seth, P., Adlakha, Y.K.: MiRNA-137-mediated modulation of mitochondrial dynamics regulates human neural stem cell fate. Stem Cells **38**(5), 683–697 (2020)
11. Song, Y., Hua, M., Zhanga, J., Teng, Z., Chen, C.: A novel mechanism of synaptic and cognitive impairments mediated via microRNA-30b in Alzheimer's disease. EBioMedicine **39**, 409–421 (2019)
12. Ardashirovaa, N.S., Fedotovaa, E.Y., Illarioshkin, S.N.: The role of microRNA in the pathogenesis and diagnostics of Parkinson's disease. Neurochem. J. **14**(2), 127–132 (2020)
13. Moghadasia, M., Alivandc, M., Fardib, M., Moghadamb, K.S., Solali, S.: Emerging molecular functions of microRNA-124: cancer pathology and therapeutic implications. Pathol. Res. Pract. **216**(3), 152827 (2020)
14. Zhdanov, V.P.: Bifurcations in the interplay of messenger RNA, protein and nonprotein coding RNA. J. Phys. A: Math. Theor. **41**(28), 285101 (2008)
15. Zhdanov, V.P.: Bistability in gene transcription: interplay of messenger RNA, protein, and nonprotein coding RNA. Biosystems **95**(1), 75–81 (2009)
16. Liu, D., Chang, X., Liu, Z., Chen, L., Wang, R., Eshel, B.J.: Bistability and oscillations in gene regulation mediated by small noncoding RNAs. PLoS ONE **6**(3), e17029 (2011)
17. Eduati, F., Di Camillo, B., Karbiener, M., Scheideler, M., Corà, D., Caselle, M., Toffolo, G.: Dynamic modeling of miRNA-mediated feed-forward loops. J. Comput. Biol. **19**(2), 188–199 (2012)
18. Zhou, P., Cai, S., Liu, Z., Wang, R.: Mechanisms generating bistability and oscillations in microRNA-mediated motifs. Phys. Rev. E **85**(4), 041916 (2012)
19. Cai, S., Zhou, P., Liu, Z.: Functional characteristics of a double negative feedback loop mediated by microRNAs. Cogn. Neurodyn. **7**(5), 417–429 (2013)
20. Nitzan, M., Shimoni, Y., Rosolio, O., Margalit, H., Biham, O.: Stochastic analysis of bistability in coherent mixed feedback loops combining transcriptional and posttranscriptional regulations. Phys. Rev. E **91**(5), 052706 (2015)
21. Mukherji, S.: Threshold response and bistability in gene regulation by small noncoding RNA. Eur. Phys. J. E **41**(1), 12 (2018)
22. Kandel, E.R., Dudai, Y., Mayford, M.R.: The molecular and systems biology of memory. Cell **157**(1), 163–186 (2014)
23. Fiumara, F., Rajasethupathy, P., Antonov, I., Kosmidis, S., Sossin, W.S., Kandel, E.R.: MicroRNA-22 gates long-term heterosynaptic plasticity in Aplysia through presynaptic regulation of CPEB and downstream targets. Cell Rep. **11**(12), 1866–1875 (2015)
24. Kandel, E.R.: The molecular dialogue biology of memory and storage: synapses between genes. Science **294**(5544), 1030–1038 (2001)
25. Liu, R.Y., Cleary, L.J., Byrne, J.H.: The requirement for enhanced CREB1 expression in consolidation of long-term synaptic facilitation and long-term excitability in sensory neurons of Aplysia. J. Neurosci. **31**(18), 6871–6879 (2011)
26. Hu, J., Adler, K., Farah, C.A., Hastings, M.H., Sossin, W.S., Schacher, S.: Cell-specific PKM isoforms contribute to the maintenance of different forms of persistent long-term synaptic plasticity. J. Neurosci. **37**(10), 2746–2763 (2017)
27. Alexandrescu, A., Carew, T.J.: Postsynaptic effects of Aplysia cysteine-rich neurotrophic factor in the induction of activity-dependent long-term facilitation in Aplysia californica. Learn. Mem. **27**(4), 124–129 (2020)
28. Frauenfelder, H., Sligar, S.G., Wolynes, P.G.: The energy landscapes and motions of proteins. Science **254**(5038), 1598–1603 (1991)
29. Wolynes, P.G., Onuchic, J.N., Thirumalai, D.: Navigating the folding routes. Science **267**(5204), 1619–1620 (1995)
30. Wang, J., Verkhivker, G.M.: Energy landscape theory, funnels, specificity, and optimal criterion of biomolecular binding. Phys. Rev. Lett. **90**(18), 188101 (2003)
31. Wang, J., Xu, L., Wang, E.: Potential landscape and flux framework of nonequilibrium networks: Robustness, dissipation, and coherence of biochemical oscillations. Proc. Natl. Acad. Sci. USA **105**(34), 12271–12276 (2008)
32. Wang, J., Li, C., Wang, E.: Potential and flux landscapes quantify the stability and robustness of budding yeast cell cycle network. Proc. Natl. Acad. Sci. USA **107**(18), 8195–8200 (2010)
33. Wang, J., Xu, L., Wang, E., Huang, S.: The potential landscape of genetic circuits imposes the arrow of time in stem cell differentiation. Biophys. J. **99**(1), 29–39 (2010)
34. Bi, Y., Yang, Z., Zhuge, C., Lei, J.: Bifurcation analysis and potential landscapes of the p53-Mdm2 module regulated by the co-activator programmed cell death 5. Chaos **25**(11), 821–829 (2015)
35. Bi, Y., Yang, Z.: Potential landscape and flux of p53-Mdm2 oscillator mediated by Mdm2 degradation rate. Int. J. Bifurcat. Chaos **26**(3), 1650042 (2016)
36. Tang, Y., Yuan, R., Wang, G., Zhu, X., Ao, P.: Potential landscape of high dimensional nonlinear stochastic dynamics with large noise. Sci. Rep. **7**, 15762 (2017)
37. Ermentrout, B.: Simulating, Analyzing, and Animating Dynamical Systems: A Guide to XPPAUT for Researchers and Students. SIAM, New Delhi (2003)

38. Guo, D., Li, C., Mei, D.C.: Switch process induced by the sine-Wiener noises in the gene transcriptional regulatory system. Physica A **525**, 1192–1202 (2019)
39. Zhu, Q.H., Shen, J.W., Ji, J.C.: Internal signal stochastic resonance of a two-component gene regulatory network under Lévy noise. Nonlinear Dyn. **100**(1), 863–876 (2020)
40. Aguda, B.D., Kima, Y., Piper-Hunterb, M.G., Friedmana, A., Marsh, C.B.: MicroRNA regulation of a cancer network: consequences of the feedback loops involving miR-17-92, E2F, and Myc. Proc. Natl. Acad. Sci. USA **105**(50), 19678–19683 (2008)
41. Siré, C., Moreno, A.B., Garcia-Chapa, M., López-Moya, J.J., Segundo, B.S.: Diurnal oscillation in the accumulation of Arabidopsis microRNAs, miR167, miR168, miR171 and miR398. FEBS Lett. **583**(6), 1039–1044 (2009)